A linear-circular regression estimate for data fusion: Application to GNSS carrier-phase signal processing

Hatchouelou Kant Williams Kouassi, Hamza Issa, Stienne Georges, Serge Reboul

Available online at www.sciencedirect.com

ScienceDirect

Digital Signal Processing 00 (2021) 1–29

www.elsevier.com/locate/procedia

A linear-circular regression estimate for data fusion: application to GNSS carrier-phase signal processing

Hatchouelou Kant Williams Kouassi*, Hamza Issa, Georges Stienne, Serge Reboul

Laboratoire d'Informatique Signal et Image de la Côte d'Opale LISIC, Université du Littoral Côte d'Opale ULCO, Calais , France

Abstract

This article is dedicated to the estimation of the parameters of a linear-circular regression model. For this model, the response is circular and defined between $-\pi$ and π, the predictor is linear and several sensors provide noisy observations of the response. In our approach, the noise is assumed to be distributed according to a von Mises distribution with a concentration parameter that models the accuracy of the sensors. We propose a maximum likelihood circular fusion operator for the estimation of the intercept, the slope of the regression line and the concentration parameter associated with each sensor. The proposed estimate is not direct as in the linear case and requires an iterative algorithm to maximize a periodic contrast function. In order to characterize the accuracy of our fusion operator, the theoretical expression of the variance of the proposed estimator slope is first derived. For this derivation, we approximate the von Mises distribution by a Wrapped normal distribution and we consider unwrapped observations. Then, we derive an iterative procedure to maximize the contrast function. We show, using synthetic data, that the variance of the slope of the regression line derived using the proposed estimate is in good agreement with that obtained using the theoretical expression of the variance. The proposed estimator is also used to process the carrier-phase difference between GNSS signals provided by two antennas. The objective in terms of signal processing is to estimate the linear parameters of this difference in order to derive the height between the two antennas. We show that fusing the observations provided by several satellite signals improves the accuracy of the estimated height. We also show, using real data, that the theoretical study of the proposed estimator can be used to predict the length of integration of the signal necessary for obtaining an estimate of the height with a given accuracy.

Keywords: Circular data processing, Information Fusion, Angular regression, GNSS carrier-phase processing

*Corresponding author.
Email addresses: hkouassi@univ-littoral.fr (Hatchouelou Kant Williams Kouassi), hamza.issa@univ-littoral.fr (Hamza Issa), georges.stienne@univ-littoral.fr (Georges Stienne), serge.reboul@univ-littoral.fr (Serge Reboul)

1. Introduction

Circular or directional data are defined on a bounded set. In this article, these data are observed as a function of time, and the interval of definition of the variables is between $-\pi$ and π. Circular data is defined in [1] as angles or points on the circumference of a unit circle with periodic measurements. In fact, the circular domain, which is indeed different from the linear domain, is of interest in the signal processing field, because several sensors can provide circular data as a function of time. In [2], observations of the direction of a moving platform (a car) are provided by a digital magnetic compass. In [3], observations of the direction of the wind are obtained with a wind vane, and in [4], with an HF radar and an anchored wave buoy. Communication systems are another domain of applications where a circular data provided by a Phase-Locked Loop (PLL) or a Phase-Open Loop (POL) is processed [5]. In robotics, directional data are processed to constitute the Direction of Arrival (DOA) obtained with acoustic sensors [6]. In imaging applications, colorimetric hue data are directional observations processed in the spatial domain [7].

Directional or circular data have been studied for a long time and the evolution of the statistical inference in this field can be observed in the following three books [8, 9, 1]. It is more recently that the signal processing community got interested in the processing of circular or directional data in the circular domain. The difference between the linear and the circular domains, such as the absence of order on the circle, indeed requires the development of new signal processing techniques. Such techniques, developed in a probabilistic framework with circular distributions, have been proposed recently. In [2, 10, 11], a recursive state filter and a fusion operator were proposed to estimate the state of a constant velocity model with circular observations of the direction. In [12], an adaptive version of the filter was proposed to process the phase provided by a POL. It also detects and corrects any abrupt changes in the signal (cycle slip). A particle filter was proposed in [13] to fuse observations of the position, defined in the linear domain, and observations of the direction, defined in the linear-circular domain, to estimate a vehicle position. In [6], a particle filter was proposed to estimate the speaker location with DOA measurements. An **Interacting Multiple Model** (IMM) filter defined in the linear-circular domain was proposed in [14] to detect maneuver with heading only observations. In [15], a von Mises Mixture Probability Hypothesis Density (PHD) filter for multi-target tracking with directional observations was proposed. The subject of this article concerns the maximum likelihood estimation of the parameters of a linear-circular regression model

in the case of multi-sensors fusion.

Multiple linear regression models fitting on a set of circular data have already been addressed in various published works. In this model, the response is an angle defined as a weighted sum of several linear predictor variables multiplied by regression coefficients. We consider the simple linear-circular model with one linear predictor variable and two regression coefficients. The response is realized with noisy angular observations defined between $-\pi$ and π. Both the response and the observations are obtained as a function of a predictor defined between $-\infty$ and $+\infty$. This model, called the "barber's pole" model, can be represented as a curve winding in an infinite number of spirals up the surface of an infinite cylinder [16]. In the linear domain, only one line can pass through two points and there is a direct estimate of the intercept and slope of the regression line. However, in the circular domain, several lines can pass through two points and there is no direct estimate of the regression line coefficients. The first iterative estimate of the linear-circular regression parameters was proposed in [16]. The proposed maximum likelihood estimate relies on the minimization of a periodic contrast function. In this case, the estimate is biased because the contrast function has several global maxima.

Johnson and Wehrly [17] proposed to map the real line to an angular interval of length 2π with a non-linear transformation, where the predictor is between $-\infty$ and $+\infty$ and the angular observations are in a single interval of length 2π. In this model, the response completes just one spiral around the cylinder as the predictor varies through its range. In this case, only one line can pass through two points of the interval. Indeed, several iterative estimates were proposed based on this approach [18, 19, 20, 21]. However, even if the contrast functions of these estimates have only one global maximum, its periodic evolution has several local maxima. The model parameter estimation requires computationally extensive optimization like Metropolis-Hastings samplings, which makes the parameter estimation extremely slow for a large data size. In practice, it is the non-linear transformation of the regression model that is fit to the observations. Therefore, this approach does not provide an estimate of the regression parameters.

A method has been proposed recently [22], to fit the observations with a mixture of linear-linear regression models. This angular Gaussian mixture model associates each spiral around the cylinder with a linear-linear model. In this approach, the number of spirals must be estimated as well as the

regression parameters. The estimation of this number is sensitive to noise and the Gaussian noise model that is used is not adapted to the processing of the transitions between $-\pi$ and π at the beginning and at the end of each interval. However, it is shown in [22] that the proposed estimator outperforms the estimates of the literature for data that follow a "barber pool" model evolution.

In this article, we propose an estimate of the linear-circular regression parameters that fuses the observations provided by several sensors. We use the classical "barber's pole" model to derive a maximum likelihood estimate for data fusion. This iterative estimate maximizes a periodic contrast function. We show, by application, that the contrast function has only one global maximum. Furthermore, we show that fusing the data provided by several sensors decreases the amplitude of the local maximum in the contrast function and improves the convergence of our estimate. Finally, we derive the variance of the estimated slope to assess, after convergence, the accuracy of the proposed estimate.

The proposed estimate is used to process a GNSS carrier-phase signal. We use an experimental setup composed of two antennas sensing two GPS signals for each satellite in view. These two signals have different trajectories and their path difference is linked to the height between the two antennas. It has been shown that the path difference can be observed through the phase delay between these two signals [23]. This phase delay, which is a function of the sine of the time varying satellite elevation, is indeed linear with a slope proportional to the height between the two antennas. In our approach, we fuse the phase delay observations obtained for several satellites in view. Furthermore, the noise power on the observed phase delay is different for each satellite due to the difference in elevation and signal propagation conditions. The estimate proposed in this article is used to fuse these observations. The theoretical accuracy of the estimate is assessed through out this experimentation. Finally, we show by experimentation, the interest of fusing the observations provided by different satellites in terms of accuracy and convergence on our iterative estimate. The performance of the proposed estimator is compared with that of the state of the art estimator described above [22]. We show that our estimator is more accurate for the estimation of the parameters of the regression in terms of standard deviation and roots mean square error.

This article is organized as follows: We introduce in the second section, the proposed fusion estimate based on the maximum likelihood. Then, the statistical properties of our estimate are

derived in the third section. In the fourth section, we assess the use of the proposed estimate for the fusion of different satellites observations in a reflectometry application using both synthetic and real data. Finally, a conclusion is provided in the fifth section.

2. Circular regression fusion

In this section, we propose a multi-sensors approach for the estimation of the parameters of a linear-circular regression model. The aim is to improve the accuracy of the estimations by using multiple sensors. In this context, it is interesting to merge the measurements provided by different sensors according to the same model into a single estimation with a lower variance. We assume the noisy measurements to be independent and distributed according to the circular normal von Mises distribution.

Let us define the following linear-circular model for one observation of the sensor s:

$$y_n^s = (\alpha + \beta\ x_n^s + \xi_n^s)\ mod\ 2\pi \tag{1}$$

where $n \in \{1, \ldots, N\}$ is the sampling instant and $s \in \{1, \ldots, S\}$ is the sensor identity. In our linear model, $\alpha + \beta\ x_n^s$, we assume that the intercept α and the slope β are the same for all the sensors. x_n^s are the deterministic, time varying predictors corresponding to the sensor s. ξ_n^s is a noise distributed according to a centered von Mises distribution. The von Mises distribution, also called Circular Normal distribution, is used for circular data in most applied problems because this distribution acts on circular data as the Normal distribution on the real line [1]. We consider the following likelihood for one observation and one sensor:

$$f(y_n^s; \alpha, \beta, \kappa^s) = \frac{1}{2\pi I_0(\kappa_s)} \exp(\kappa^s \cos(y_n^s - (\alpha + \beta\ x_n^s))) \tag{2}$$

where κ^s is the concentration parameter of the Von Mises distribution. I_0 is the modified Bessel function of the first kind and order zero. Let us define the vector Y of N measurements coming from S sensors:

$$Y = \left\{y_1^1, \ldots, y_N^1, \ldots, y_1^S, \ldots, y_N^S\right\} \tag{3}$$

In this article, we assume that the measurements are independent. This point will be discussed again in section 4.2.4. for our application on GNSS carrier-phase signal processing.

The likelihood of these $N \times S$ measurements is given by:

$$L(Y) = f(y_1^1; \alpha, \beta, \kappa^1) \dots f(y_N^S; \alpha, \beta, \kappa^S) \tag{4}$$

Then:

$$L(Y) = \prod_{s=1}^{S} \prod_{n=1}^{N} \frac{1}{2\pi I_0(\kappa_s)} \exp(\kappa^s cos(y_n^s - (\alpha + \beta\ x_n^s))) \tag{5}$$

We derive the log of the likelihood function as:

$$\ln(L(Y)) = \sum_{s=1}^{S} \sum_{n=1}^{N} \kappa^s \cos(y_n^s - (\alpha + \beta\ x_n^s)) - N \sum_{s=1}^{S} \ln(2\pi I_0(\kappa_s)) \tag{6}$$

In order to define the estimate $\hat{\beta}$ of the slope β (in the whole article, the notation $\hat{.}$ corresponds to the estimate of a parameter), we maximize the log of the likelihood using the following contrast function:

$$W(Y) = \sum_{s=1}^{S} \sum_{n=1}^{N} \hat{\kappa}^s \cos(y_n^s - (\hat{\alpha} + \hat{\beta}\ x_n^s)) \tag{7}$$

In the following, we first present the direct maximum likelihood estimate of κ^s (resp. α), assuming that α and β (resp. κ^s and β) are known. $\hat{\alpha}$ and $\hat{\kappa}^s$ are thus defined as functions of $\hat{\beta}$. We then propose in a second step an iterative estimate of β.

It is shown in [1] that, for a von Mises distribution of the noise, the maximum likelihood estimate of κ^s is obtained with the following expressions when α and β are known:

$$\frac{\partial ln(L(Y))}{\partial \kappa^s} = \sum_{n=1}^{N} \cos(y_n^s - (\alpha + \beta\ x_n^s)) - N \frac{I_1(\kappa^s)}{I_0(\kappa^s)} = 0 \tag{8}$$

with $I_1(\kappa^s) = \partial(I_0(\kappa^s))/\partial\kappa^s$ the modified Bessel function of the first kind and order one. Then, we can define $A(\kappa^s)$ as:

$$A(\kappa^s) \triangleq \frac{I_1(\kappa^s)}{I_0(\kappa^s)} = \frac{1}{N}\sum_{n=1}^{N}\cos(y_n^s - (\alpha + \beta\ x_n^s)) \tag{9}$$

The maximum likelihood estimate of κ^s is thus obtained by:

$$\hat{\kappa}^s = A^{-1}\left(\frac{\sum_{n=1}^{N}\cos(y_n^s - (\alpha + \beta\ x_n^s))}{N}\right) \tag{10}$$

According to [1], $A(\kappa^s)$ is a strictly monotone increasing function of κ^s so $\hat{\kappa}^s$ is the unique solution to equation (10). There are different methods defined in [24] for the processing of the non linear function A^{-1} which includes the Runge-Kutta method, the Newton method and the Taylor expansion method. In this article, we use the Runge-Kutta method for the estimation of A^{-1}.

The maximum likelihood estimate $\hat{\alpha}$ is obtained with the nil value of the first derivative of $W(Y)$, assuming that κ^s and β are known. Thus, we have:

$$\frac{\partial W(Y)}{\partial\alpha} = 0 \ \text{ then } \ \sum_{s=1}^{S}\sum_{n=1}^{N} -\kappa^s \sin(y_n^s - (\hat{\alpha} + \beta\ x_n^s)) = 0 \tag{11}$$

With:

$$\cos(\hat{\alpha})\sum_{s=1}^{S}\sum_{n=1}^{N}\kappa^s \sin(y_n^s - \beta\ x_n^s) - \sin(\hat{\alpha})\sum_{s=1}^{S}\sum_{n=1}^{N}\kappa^s \cos(y_n^s - \beta\ x_n^s) = 0 \tag{12}$$

Therefore, we derive $\hat{\alpha}$ as:

$$\hat{\alpha} = arctan^*\left(\frac{\sum_{s=1}^{S}\sum_{n=1}^{N}\kappa^s \sin(y_n^s - \beta\ x_n^s)}{\sum_{s=1}^{S}\sum_{n=1}^{N}\kappa^s \cos(y_n^s - \beta\ x_n^s)}\right) \tag{13}$$

Where $arctan^*$ is the "quadrant specific" inverse of the tangent. It is shown in [2] that this expression of $\hat{\alpha}$ provides a negative value for the second derivative of $W(Y)$ (and thus a maximum of $W(Y)$).

In expression (13) β and κ^s are assumed to be known. For this expression, a change in the value of β affects both the variance and the mean value of $\hat{\alpha}$. A change in the value of κ_s only affects the variance of the estimate of α, because (13) is the weighted sum of $(y_n^s - \beta x_n^s)$ with weights κ^s [2].

In this context, the mean value of the estimate of α only depends on β. Consequently, the mean value of the estimate of κ^s only depends on β.

There is no direct estimate of β associated with the contrast function $W(Y)$. In order to find the value $\hat{\beta}$ that maximize the likelihood, we use the iterative Newton-Raphson [25] algorithm to maximize the contrast function $W(Y)$. Then we have the following:

$$\hat{\beta}^{i+1} = \hat{\beta}^i + \left(\frac{\partial^2 W(Y)}{\partial \beta^2}\right)^{-1} \left(\frac{\partial W(Y)}{\partial \beta}\right)|_{\beta=\hat{\beta}^i} \tag{14}$$

and:

$$\left(\frac{\partial W(Y)}{\partial \beta}\right) = \sum_{s=1}^{S}\sum_{n=1}^{N} x_n^s \kappa^s \sin(y_n^s - (\alpha + \beta\ x_n^s)) \tag{15}$$

$$\left(\frac{\partial^2 W(Y)}{\partial \beta^2}\right) = \sum_{s=1}^{S}\sum_{n=1}^{N} (x_n^s)^2 \kappa^s \cos(y_n^s - (\alpha + \beta\ x_n^s)) \tag{16}$$

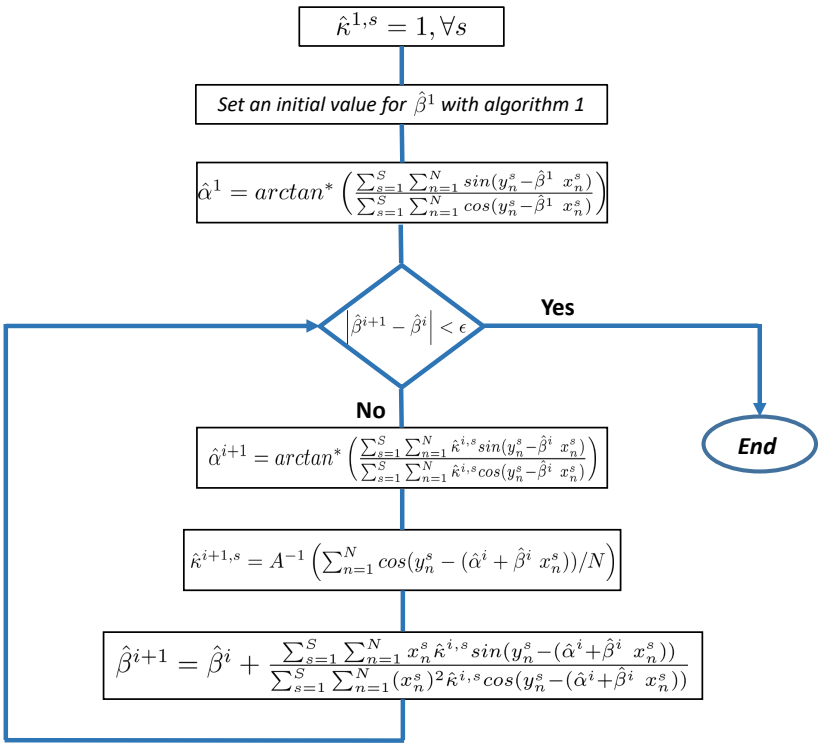

Fig. 1: Flowchart of the iterative estimation of the parameters

The pseudo-code of the proposed iterative estimate method is given in the flowchart described in Figure 1. We present in Algorithm 1 the initialization of $\hat{\beta}^1$.

In Figure 1, ϵ is the stopping criterion of the algorithm. Its value defines the accuracy of our estimate and will be fixed in section 4 in the context of our application. In order to characterize the proposed iterative estimate, we derive in section 3.1 the theoretical performance of the Maximum Likelihood Estimate and we discuss in section 3.2 the convergence of the proposed iterative estimate.

Data: Noisy observations: $y_n^s \ \forall s \in \{1,\dots,S\} \ \forall n \in \{1,\dots,N\}$.

Model parameters: N, S, $x_n^s \ \forall s \in \{1,\dots,S\} \ \forall n \in \{1,\dots,N\}$.

Algorithm parameters: research step p, β_{max} maximum value for $\hat{\beta}^1$.

Result: initial value $\hat{\beta}^1$

Initialization :

Set $\hat{\kappa}^s = 1 \ \forall s \in \{1,\dots,S\}$

Algorithm :

for β_r ranging from 0 to β_{max} by steps of p

$\hat{\alpha} \leftarrow arctan^* \left(\frac{\sum_{s=1}^{S} \sum_{n=1}^{N} \sin(y_n^s - \beta_r \ x_n^s)}{\sum_{s=1}^{S} \sum_{n=1}^{N} \cos(y_n^s - \beta_r \ x_n^s)} \right)$

$W(\beta_r) \leftarrow \sum_{s=1}^{S} \sum_{n=1}^{N} \kappa^s \cos(y_n^s - (\hat{\alpha} + \beta_r \ x_n^s))$

endfor

$\hat{\beta}^1 = \underbrace{argmax}_{\beta_r}(W(\beta_r))$

return $\hat{\beta}^1$

Algorithm 1: Setting of an initial value of $\hat{\beta}$

3. Theoretical performance and convergence conditions

3.1. Estimator accuracy and Cramer-Rao Lower Bound

The objective of this section is to derive the variance of the Maximum Likelihood Estimate (MLE) of β and the Cramer-Rao Lower Bound (CRLB) on the variance of the unbiased estimation of β. In our development, we first derive the variance and the CRLB of β in the presence of a single sensor, then we extend the result to the multi-sensors scenario.

For this aim, we apply two approximations in order to obtain the derivative of the likelihood function. In this regard, we consider unwrapped circular data in our model. Furthermore, the highly non-linear von Mises distribution is approximated with a Wrapped normal distribution. These two approximations are validated in the next section using synthetic data. Let us define the following model expression:

$$y_n^s = \alpha + \beta\ x_n^s + \xi_n^s \tag{17}$$

We approximate the von Mises distribution by a Wrapped Normal distribution. According to the unwrapped data model, the Wrapped Normal distribution of an observation is defined as:

$$f(y_n^s; \alpha, \beta, \sigma^s) = \frac{1}{\sigma^s\ \sqrt{2\pi}} \sum_{k=-\infty}^{\infty} \exp\left(-\frac{(y_n^s - \alpha - 2k\pi - \beta\ x_n^s)^2}{2(\sigma^s)^2}\right) \tag{18}$$

It is shown in [1] that the Von Mises distribution of concentration parameter κ^s can be approximated by a Wrapped normal distribution with a variance $(\sigma^s)^2$. The link between these two distributions is given by the following expression:

$$(\sigma^s)^2 \approx -2ln(A(\kappa^s)) \tag{19}$$

with lower precision losses for large $(\sigma^s)^2$ values.

Considering N measurements of sensor s, and thus $Y^s = \{y_1^s, ..., y_N^s\}$, the likelihood of the observations is given by :

$$\begin{aligned} L(Y^s) &= f(y_1^s; \alpha, \beta; \sigma^s), ..., f(y_N^s; \alpha, \beta; \sigma^s) \\ &= \left(\frac{1}{\sigma^s\ \sqrt{2\pi}}\right)^N \sum_{k=-\infty}^{\infty} \exp\left(-\frac{1}{2(\sigma^s)^2} \sum_{n=1}^{N} (y_n^s - \alpha - 2k\pi - \beta\ x_n^s)^2\right) \end{aligned} \tag{20}$$

We derive in Appendix A the MLE of β in the mono-sensor and multi-sensors cases.

Let Y_n^s be a random variable distributed according to a Wrapped normal distribution, and y_n^s be a realization of Y_n^s. Then, we can derive the variance of the estimate of β as a function of

$var(Y_n^s) = (\sigma^s)^2$ in the mono-sensor case as:

$$var(\hat{\beta}) = var\left(\sum_{n=1}^{N}(N\ y_n^s\ x_n^s) - \sum_{n=1}^{N} y_n^s\ \sum_{n=1}^{N} x_n^s\right)\ \frac{1}{\left(\sum_{n=1}^{N} N\ (x_n^s)^2 - \left(\sum_{n=1}^{N} x_n^s\right)^2\right)^2}$$

Then, we have:

$$var(\hat{\beta}) = (\sigma^s)^2 \frac{\sum_{n=1}^{N}(N\ x_n^s)^2 - N\left(\sum_{n=1}^{N} x_n^s\right)^2}{\left(\sum_{n=1}^{N} N\ (x_n^s)^2 - \left(\sum_{n=1}^{N} x_n^s\right)^2\right)^2}$$

Finally:

$$var(\hat{\beta}) = \frac{-2ln(A(\kappa^s))}{\sum_{n=1}^{N}\left(x_n^s - \overline{x^s}\right)^2} \tag{21}$$

where $\overline{x^s} = \frac{1}{N}\sum_{n=1}^{N} x_n^s$.

The expression of the MLE $\hat{\beta}$ (equation (A.4)) and its variance are the same as in the linear domain for data following a Normal distribution. Consequently, like for such data, the expression of the obtained variance of the MLE (equation (21)) is also the CRLB for the unbiased estimation of β. With a similar demonstration, when the value of α is known and not to be estimated, expression (21) becomes :

$$var(\hat{\beta}) = \frac{-2ln(A(\kappa^s))}{\sum_{n=1}^{N}(x_n^s)^2} \tag{22}$$

where (22) is also the CRLB for the unbiased estimation of β. In the multi-sensors case, the MLE of β (equation (A.5)) is, as in the linear case, the weighted sum fusion operator that minimizes the variance of $\hat{\beta}$. According to [26], we thus have:

$$var(\hat{\beta}) = \frac{1}{\sum_{s=1}^{S}\sum_{n=1}^{N}\frac{(x_n^s - \overline{x})^2}{-2ln(A(\kappa^s))}} \tag{23}$$

where $\overline{x} = \frac{1}{NS}\sum_{s=1}^{S}\sum_{n=1}^{N} x_n^s$.

When α is known:

$$var(\hat{\beta}) = \frac{1}{\sum_{s=1}^{S}\sum_{n=1}^{N}\frac{(x_n^s)^2}{-2ln(A(\kappa^s))}} \tag{24}$$

Equations (23) (resp. (24)) expresses the CRLB for the unbiased estimation of β in the multi-sensors case when α is unknown (resp. known). In the experimentation section, we assess the proposed variance estimates with angular observations generated with a linear-circular regression model.

3.2. Convergence conditions for the proposed iterative estimate

The proposed iterative estimate described in Figure 1 relies on a Newton-Raphson algorithm that maximizes expression (7). $W(Y)$, the contrast function defined in expression (7), is a periodic function of β with several global maxima. We show in this section that when $x_n \in [0,\ 1]$ it can be assumed that there is only one single global maximum. However, expression (7) has several local maxima. We discuss in this section the conditions of convergence of the proposed estimate in such case. We have:

$$\hat{\beta} = \underbrace{argmax}_{\tilde{\beta}} W(Y) \tag{25}$$

In this expression and in the remainder of the paper, the notation $\tilde{.}$ corresponds to the values obtained when exploring the possible values of β that maximizes $W(Y)$.

$$W(Y) = \sum_{s=1}^{S}\sum_{n=1}^{N} \cos(y_n^s - (\tilde{\alpha} + \tilde{\beta}x_n^s)) \tag{26}$$

$$= \sum_{s=1}^{S}\sum_{n=1}^{N} \cos(\alpha - \tilde{\alpha} + \beta x_n^s - \tilde{\beta}x_n^s + \xi_n^s) \tag{27}$$

In the preceding expression of $W(Y)$, the global maxima are immersed in noise. In order to characterize these global maxima, we consider the unnoisy expression $\tilde{W}(Y)$. **In this expression, $\tilde{\alpha}$ is a function of $\tilde{\beta}$ according to expression (13).** Then we have:

$$\tilde{W}(Y) = \sum_{s=1}^{S}\sum_{n=1}^{N} \cos(\alpha - \tilde{\alpha}(\tilde{\beta}) + x_n^s(\beta - \tilde{\beta})) \tag{28}$$

where x_n^s are increasing numbers with n, s. In expression (28) if $\tilde{\beta} = \beta$ then $\tilde{\alpha} = \alpha$ and $\tilde{W}(Y)$ is maximum and equal to $N \times S$. We define:

$$\frac{x_1^1}{x_n^s} = \frac{k_1^1}{k_n^s}\ \forall n, s$$

where k_1^1/k_n^s is the fraction of the rational number x_1^1/x_n^s and the set of values $\left\{k_1^1, \ldots, k_N^S\right\}$ are integers simplified by their greatest common divisor.

For :

$$\tilde{\beta} \quad = \quad \beta + 2\pi \frac{k_1^1}{x_1^1} \tag{29}$$

We have, according to expression (13):

$$\tilde{\alpha}(\tilde{\beta}) = arctan^* \left(\frac{\sum_{s=1}^{S} \sum_{n=1}^{N} \kappa^s \sin(\alpha + \beta\ x_n^s - (\beta + 2\pi \frac{k_1^1}{x_1^1})\ x_n^s)}{\sum_{s=1}^{S} \sum_{n=1}^{N} \kappa^s \cos(\alpha + \beta\ x_n^s - (\beta + 2\pi \frac{k_1^1}{x_1^1})\ x_n^s)} \right) = \alpha \tag{30}$$

and expression (28) becomes:

$$\tilde{W}(Y) \quad = \quad \sum_{s=1}^{S} \sum_{n=1}^{N} \cos(-2\pi x_n^s \frac{k_1^1}{x_1^1}) \tag{31}$$

$$= \quad \sum_{s=1}^{S} \sum_{n=1}^{N} \cos(-2\pi k_n^s) \tag{32}$$

In this case $\tilde{W}(Y)$ is maximum and equal to $N \times S$.

Let us consider the case of our application where $x_n^s \in [0, 1]$. The value of x_n^s is obtained with a floating-point data type which has a mantissa of 15 elements. The value k_1^1 is thus equal to $fix(x_1^1 \times e15)$, where the function $fix()$ rounds the elements toward zero, resulting in an integer. The difference between two estimates of β associated with two global maxima of $\tilde{W}(Y)$ is obtained with expression (29). This difference is equal to $\frac{2\pi k_1^1}{x_1^1} = 6.28e15$ (for example $\frac{k_1^1}{x_1^1} = \frac{76024...}{0,76024...} = 1e15$). This high value guarantees a second global maximum outside the search window of our application.

However, expression (7) has several local maxima in the search window that may influence the convergence of the proposed iterative estimate. The algorithm converges if the initial value $\hat{\beta}^1$ is positioned on the peak of the global maximum. In practice, due to the presence of noise, the initial value $\hat{\beta}^1$ can be positioned on a local maximum peak. In this case the estimate of beta can be far

from its true value. In order to ensure the convergence of the estimate, the number N of samples from each sensor and/or the number S of sensors can be increased.

In section 4.2, we simulate a real application context and define the minimum value of N according to different multi-sensors configurations. We show that the number of samples N necessary for the variance of the proposed estimate to reach the CRLB bound gets lower when the number of sensors S is higher.

4. Experimentation

4.1. Model assessment on synthetic data

In this section, we study the properties of the proposed estimate in the unbiased case as defined in section 3.1. The aim is to assess the theoretical expressions of $var(\hat{\beta})$ using synthetic data. For this purpose, we compare the theoretical values of $var(\hat{\beta})$ obtained with the expressions derived in section 3.1 with the results obtained by simulation. Two signals following the linear-circular regression model defined in equation (1) are processed in the simulation. The two signals are sampled with a sampling frequency of $1000Hz$ over a period of $1s$. In order to evaluate the fusion operator, each signal is generated with different realizations of the von Mises noise process defined by κ^s. We consider two sensors providing the two signals with a noise power defined as κ^1 and κ^2. To process the variance of the estimate of β, 1000 realizations of both signals are used. In this simulation, the values of α and β are arbitrarily fixed to $\frac{\pi}{4}$ and 15 respectively. The stopping criterion ϵ of the iterative algorithm described in Figure 1 is fixed to $1e-5$ in order to estimate the parameters with the millimeter accuracy. The research step p defined in Algorithm 1 for setting an initial value of $\hat{\beta}$ is fixed to 10^{-2}. Both signals share the same predictor x_n^s corresponding to the sampled time values varying from 0 to $1s$ with a step of $1ms$. In this context the convergence of the proposed iterative estimate is guaranteed.

We report in Table 1, the values of $var(\hat{\beta})$ as a function of the noise power (different values of κ) for each signal when α is unknown and to be estimated. In this table, we process the theoretical values (Theo) of $var(\hat{\beta})$, proved in section 3.1 to also be the CRLB for the unbiased estimation of β, obtained with expressions (21) and (23), and the simulated values (Sim) obtained using the

algorithm defined in Figure 1. We report $var(\hat{\beta})$ for each signal separately (mono-sensor regression) and when the two signals are fused together (multi-sensors regression).

Table 1: Assessment of $var(\hat{\beta})$ when α is unknown. We report the theoretical values (Theo) obtained with expressions (21) and (23), and the practical values obtained by simulation using the algorithm from Figure 1 (Sim). **The values in this table are factors of** 10^{-4}.

		var($\hat{\beta}$) signal 1		var($\hat{\beta}$) signal 2		var($\hat{\beta}$) Fusion	
κ^1	κ^2	Theo	Sim	Theo	Sim	Theo	Sim
1	1	192.9	269.1	192.9	270.3	96.4	134.7
1	2	192.9	276.1	86.1	82.3	59.5	59.7
3	4	50.4	49.1	35.1	32.1	20.6	20.4
5	5	26.9	29.5	26.9	28.1	13.4	12.9
5	15	26.9	27.6	8.3	8.4	6.3	6.8

We notice in Table 1 that the results obtained with the theoretical model are close to those obtained by simulation when $\kappa^1 \geq 2$ and $\kappa^2 \geq 2$. This is due to the fact that the approximation of a von Mises distribution by a Wrapped normal distribution performs poorly when $\kappa < 2$ [1]. In addition, by comparing the theoretical (Column 5) and simulation (Column 6) results in the case of multi-sensors regression (fusion of both signals), we notice that the values are indeed very close. Therefore, we can conclude that the proposed fusion operator in the circular domain, is the weighted sum of the observations, as in the linear domain. The theoretical expression of $var(\hat{\beta})$ is indeed derived for a weighted sum of the observations. Finally, Table 1 shows that the proposed estimate in the circular domain, has the same properties as that in the linear domain. We can indeed observe an improvement in the estimate's accuracy when κ increases and when the data are fused.

We report in Table 2, the values of $var(\hat{\beta})$ when α is known. In this context, only β and κ^s are estimated with the algorithm defined in Figure 1. The estimation of β is assessed for different noise powers (different values of κ) on each signal. We process the theoretical values of $var(\hat{\beta})$ (equal to the CRLB for the unbiased estimation of β according to section 3.1) obtained with expressions (22) and (24) and the $var(\hat{\beta})$ values obtained by simulation using the iterative algorithm. We report

$var(\hat{\beta})$ for each signal and for the fusion of the two signals.

Table 2: Assessment of the expression $var(\hat{\beta})$ when α is known. We report the theoretical values (Theo) obtained with expressions (22) and (24), and the practical values obtained by simulation using the algorithm from Figure 1 (Sim). **The values in this table are factors of** 10^{-4}.

		var($\hat{\beta}$) signal 1		var($\hat{\beta}$) signal 2		var($\hat{\beta}$) Fusion	
κ^1	κ^2	Theo	Sim	Theo	Sim	Theo	Sim
1	1	48.3	69.1	48.3	62.1	24.1	35.9
1	2	48.34	69.5	21.5	21.8	14.9	15.8
3	4	12.6	12.4	8.7	8.7	5.2	5.1
5	5	6.8	6.9	6.8	6.8	3.3	3.5
5	15	6.7	7.1	2.1	2.1	1.6	1.7

Similar to Table 1, the results reported in Table 2 show that the theoretical model is close to the simulation when $\kappa^1 \geq 2$ and $\kappa^2 \geq 2$. The difference obtained for $\kappa < 2$ can be explained using the same reasoning as above. The large difference between the results obtained in Table 1 and Table 2 are explained by the fact that the knowledge of α increases the accuracy in the estimation of β (see equations (21),(22) and (23),(24)).

According to the results of Table 1 and Table 2, we observe that the estimation of $\hat{\kappa}^s$ in the algorithm defined in Figure 1 doesn't significantly affect the estimation of $var(\hat{\beta})$. The theoretical value of $var(\hat{\beta})$, that uses the true value of κ^s, is indeed close to the simulation which uses an estimate of $\hat{\kappa}^s$. Thus, the theoretical value isn't affected by errors in the estimation of κ^s.

4.2. Application to GNSS carrier-phase signal processing

In this section, we use the theoretical results derived in section 3.1 to assess the proposed regression model to process a GNSS carrier-phase signal. We evaluate the accuracy of the estimator for calculating the height between two GNSS antennas.

4.2.1. Problem statement

Figure 2 presents the experimental setup. The setup is composed of two antennas linked to a two channel GNSS receiver. It can be shown that the height h between the two antennas is linked to δ^s, the path difference between the two signals.

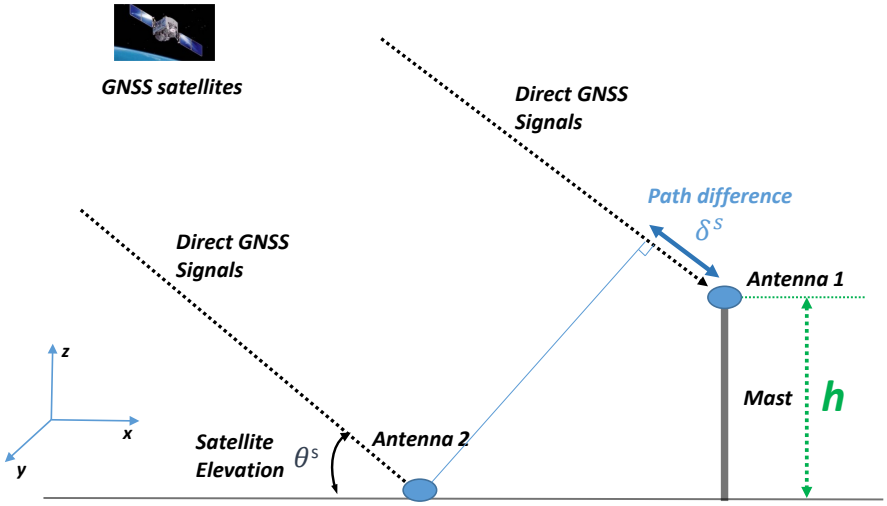

Fig. 2: Geometry of the experimental setup

In the digital case, the model expression corresponding to the phase difference is given by [23]:

$$y_n^s = \left(\frac{4\pi}{\lambda} \; h \; \sin\theta_n^s + \xi_n^s \right) mod(2\pi) \tag{33}$$

where $\lambda = 19.04 \; cm$ is the wave length corresponding to the GPS-L1 frequency.

Compared to the linear-circular model defined in equation 1, the intercept $\alpha = 0$ is known, the slope β is equal to $\frac{4\pi}{\lambda} \; h$ with h unknown, $x_n^s = \sin\theta_n^s$ are the predictors for each satellite and ξ_n^s are additional noises following a von Mises distribution [27]. The von Mises distribution is centered and its concentration parameter κ^s models the noise power on the observations of carrier-phase for each GNSS satellite s. h, the height to estimate, is derived from the estimate of β. As before, we use $p = 10^{-2}$ for the initialization of $\hat{\beta}$. The elevation θ_n^s is derived from the GNSS satellite ephemeris and from the antenna position. According to the model of [23], we assume that we accurately know

the relative positions of the antennas in the horizontal (x, y) plane. This assumption fits only for a rigid experimental setup.

In this evaluation, we use a satellite constellation obtained in the 5th of June 2018 at 8h33'18" UTC. The visible satellites are obtained from a GNSS antenna ($50.953228°N$; $1.880285°E$) situated on the roof of the LISIC (Laboratoire d'Informatique Signal et Image de la Côte d'Opale). The satellite elevations are processed based on a RINEX file provided by a NovAtel OEM7 receiver. We show in Figure 3, a sky-plot of the satellite constellation.

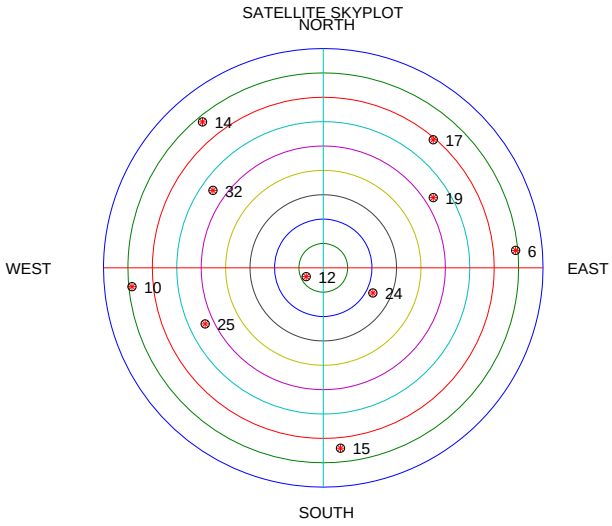

Fig. 3: Constellation of the visible GPS satellites obtained with the NovAtel receiver

In the next section, we assess the estimation of h in terms of accuracy for a given satellite constellation. We report in Table 3, the concentration parameter κ of the von Mises noise distribution on the observations of carrier-phase corresponding to different carrier-to-noise ratio (C/N_0) values of a GPS signal.

Table 3: Carrier-to-noise ratio (C/N_0) of a GPS signal and the corresponding concentration parameter (κ) of the von Mises noise distribution on the observations of carrier-phase.

C/N_0 **(dB.Hz)**	30	35	40
κ	1.35	2.96	9.34

We show in Figure 4, a simulation of noisy phases corresponding to two satellites. We can observe on this figure that the satellites provide different elevations and noise powers.

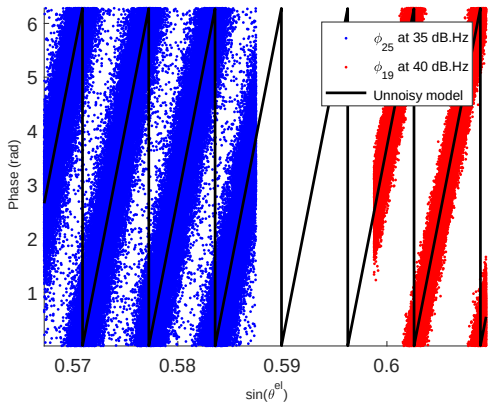

Fig. 4: Simulation of noisy carrier-phase measurements for two satellites

The proposed estimate fuses the phase observations provided by several satellites with different elevations. The aim is to show that the fusion improves the accuracy of the estimation.

4.2.2. Assessment of the estimator accuracy

We report different satellite constellation configurations in Table 4. We propose to evaluate our estimator for the East, West, South-West, and the North-East sides of the satellites skyplot as well as the whole constellation (the four quadrants). We study in Table 4 the influence of the considered satellite constellation, which defines the multi-sensors configuration of the proposed estimate. We sort the visible satellites as a function of the increasing elevation to fit the theoretical model. In this table, we report the difference of height Δh between two successive global maxima in $\tilde{W}(Y)$. This height is processed with one observation per satellite ($N = 1$). We also report the height of the highest local maximum in the search window, as a percentage of the global maximum height.

For this application, the search window for the height to be retrieved is set between 0 m and 100 m. The height used in this simulation is set to 15 m.

Table 4: Assessment of the proposed estimate as a function of the satellite constellation. We report the difference of height Δh and the highest local maximum other than the global one in the search window which is normalized with respect to the global maximum.

Satellite constellation	Δh (m)	Local maximum height	Satellite PRNs and elevations
West side	9.52e13	0.789	14 (10°),10 (12°),32 (33°), 25 (34°), 12 (80°)
East side	9.52e13	0.834	6 (9°), 15 (17°), 17 (22°), 19 (37°), 24 (69°)
North-East side	4.76e13	0.973	6 (9°), 17 (22°),19 (37°)
South-West side	9.52e13	0.977	10 (12°), 25 (34°), 12 (80°)
Four quadrants	9.52e13	0.628	All visible satellites

The values of the second column of Table 4 show that the second maximum of $\tilde{W}(Y)$ is very far from the search window. Thus, we can conclude that the contrast function $W(Y)$ of the proposed estimate has a single global maximum in the search window. When considering only the North-Eastern satellites, the value of Δh is smaller because 2 is a common divisor for k_1^1, k_1^2 and k_1^3. We show in Column 3 of Table 4, that the height of the local maximum decreases with the increase

in the number of satellites S. We can conclude that multi-sensors (multi-satellites) fusion improves the proposed iterative estimate by increasing the difference between the global maxima of $\tilde{W}(Y)$ and the local maxima.

Unfortunately, the proposed estimate accuracy never reaches the CRLB if the SNR of $W(Y)$ does not allow to differentiate the global maximum from the local maxima. For a given multi-sensors (multi-satellites) configuration, the only way to improve the SNR is to increase the period of integration N. In this context, we report in Table 5, the minimum period of integration N necessary for the proposed MLE of h to reach the CRLB as a function of the satellite constellation and the carrier-to-noise ratio C/N_0. We also report the CRLB of the MLE of h, noted $CRLB(\hat{h})$ and the simulated standard deviations $STD(\hat{h})$ of the unbiased estimation of h.

In Table 5, the estimate is supposed to have converged towards the global maximum when the value of $STD(\hat{h})$ obtained by 1000 successive simulations is close to the value of $CRLB(\hat{h})$. Column 2 of Table 5 represents the minimum period of integration N. Thus, N can be seen as the convergence rate of our estimate. In each quadrant of the satellite constellation, we observe that the period of integration increases when C/N_0 decreases (the SNR of $W(Y)$ decreases). Furthermore, by comparing Table 5 and Table 4, we deduce that the period of integration of the signal N in ms increases with the increase in the normalized local maximum of $\tilde{W}(Y)$.

In Columns 4 and 5 of Table 5, one can observe that best performance of the estimator in terms of integration time is reported for the four quadrants (whole constellation) followed by the West and East sides of the constellation. The decrease in the integration period is due to the increase in the number of visible satellites. On the other hand, we can observe that the best performances of the estimator in terms of standard deviation are reported for the North-East and the South-West sides. This is due to the fact that the integration time and overall number of observations considered for the estimation of the parameters is higher. For similar integration times, the two quadrants and four quadrants constellations would provide lower standard deviations than the North-East and South-West ones. Therefore, we conclude that the proposed estimate converges when we fuse observations from several satellites for a sufficient integration period. This period of integration decreases with the increase in the number of satellites.

Table 5: Assessment of the integration time necessary for the proposed MLE of h to reach the CRLB, as a function of the satellite constellation and C/N_0. In this table, we also report the CRLB and the simulated standard deviation $STD(\hat{h})$ of the proposed MLE of h.

Satellite constellation	C/N_0 (dB.Hz)	Integration (ms)	$CRLB(\hat{h})$ (cm)	$STD(\hat{h})$ (cm)	Satellites PRN and elevation
West side	40	17	0.10	0.10	14 (10°),10 (12°),32 (33°), 25 (34°), 12 (80°)
	35	25	0.15	0.17	
	30	60	0.16	0.17	
East side	40	19	0.10	0.10	6 (9°), 15 (17°), 17 (22°), 19 (37°), 24 (69°)
	35	30	0.15	0.13	
	30	72	0.16	0.16	
North-East side	40	100	0.07	0.06	6 (9°), 17 (22°),19 (37°)
	35	160	0.11	0.10	
	30	500	0.10	0.12	
South-West side	40	140	0.03	0.04	10 (12°), 25 (34°), 12 (80°)
	35	500	0.03	0.04	
	30	950	0.04	0.05	
Four quadrants	40	9	0.10	0.10	All visible satellites
	35	11	0.17	0.18	
	30	15	0.24	0.27	

4.2.3. Comparison with a state-of-art method

We report in Table 6 the standard deviation and the root mean square error of the estimation of h obtained using a state of the art estimator [22] and the estimator proposed in this article. In Table 6, columns 5 and 7 show the standard deviation and the root means square values obtained using the state of the art estimator, for 1000 successive simulations. These results are obtained using an Expectation-Maximization (EM) algorithm with the same initialization of $\hat{\beta}$ as defined in the proposed algorithm (Figure 1). We use, for both algorithms, the same integration time that

has been defined in Table 5. By comparing columns 5 and 7, we notice that the state of the art estimator is biased. This estimator indeed overestimates the height between the two antennas by an average of 1 cm to 6 cm depending on the considered satellite constellation and noise level. Furthermore, columns 4 and 6 show that the estimator proposed in this article is unbiased for the considered integration times and that it is also more accurate than the state of the art estimator in terms of standard deviation by factors of 1 to 3 approximately.

Table 6: Standard deviation $STD(\hat{h})$ and root mean square error $RMSE(\hat{h})$ of the estimation of h for the estimator presented in this article (Prop) and for a state of the art estimator (SotA) [22].

Satellite constellation	C/N_0 (dB.Hz)	Integration (ms)	$CRLB(\hat{h})$ Prop(cm)	$STD(\hat{h})$ SotA(cm)	$RMSE(\hat{h})$ Prop(cm)	$RMSE(\hat{h})$ SotA(cm)
West side	40	17	0.10	0.20	0.10	3.74
	35	25	0.17	0.28	0.17	3.14
	30	60	0.17	0.24	0.17	2.46
East side	40	19	0.10	0.34	0.10	3.78
	35	30	0.13	0.41	0.13	3.04
	30	72	0.16	0.27	0.16	2.55
North-East side	40	100	0.06	0.15	0.06	1.01
	35	160	0.10	0.20	0.10	2.09
	30	500	0.12	0.12	0.12	2.83
South-West side	40	140	0.04	0.09	0.04	5.96
	35	500	0.04	0.08	0.04	5.25
	30	950	0.05	0.07	0.05	4.33
Four quadrants	40	9	0.10	0.27	0.10	3.75
	35	11	0.18	0.39	0.18	3.09
	30	15	0.27	0.38	0.27	2.51

4.2.4. Assessment on real data

In this section, we assess the proposed estimate on real data. We use the experimental setup of Figure 2 to assess the proposed estimate, because the geometry parameters are accurately known (we accurately know the relative positions of the antennas in the horizontal (x, y) plane) and the whole satellite constellation can be used.

With this setup, we observe the carrier-phases of all the satellites in view. We report in Table 7, the elevations of the visible satellites. The raw data concerning the GNSS signals are recorded using an L1-L5 Syntony bit grabber. A GNSS software receiver developed by the LISIC is used to estimate the parameters of the signals using a Delay-Locked Loop (DLL), a Phase-Locked Loop (PLL) and a Frequency-Locked Loop (FLL). The satellites elevations and signal timing are obtained from this software receiver by processing the received GNSS data messages.

The height h between the two antennas is processed with the proposed multi-sensors regression estimate. The value of h in the experimental setup is approximately 53 cm.

Table 7: Satellites elevations. (Sept. 3 2020, 13h12 UTC).

PRN	25	10	6	19	12	14	15	24	17	32
θ_n^s (°)	34.55	12.50	9.75	37.55	80.00	10.73	17.50	69.24	22.20	33.39

For the satellites elevations presented in Table 7, the normalized height of the local maximum of $\tilde{W}(Y)$ is 0.603. Applying the same approach as that presented in Table 5, we expect the estimate to be unbiased after 9 ms of signal integration. For this length of integration and this satellite configuration, the theoretical standard deviation of the estimate of h is 2 mm.

We report in Table 8, the estimate of h processed using GPS-L1 C/A signals acquired on several days of the same month (September 2020). The signals were recorded at approximately the same hour of each day in order to always observe the same satellite constellation, with elevations close to those presented in Table 7. Two integration periods are considered: 9 ms, corresponding to the minimum theoretical period defined in Table 5, and 20 ms, which is an integration period commonly used in GPS-L1 receivers corresponding to the duration of a data bit.

Table 8: Day of month (September 2020), time (UTC), and the estimates of h over 9 days. The estimates of h are given for two periods of integration, 9 ms and 20 ms.

Day of month	03	04	07	08	10	11	12	14	17
Time (UTC)	13h12	13h15	13h14	13h12	13h11	13h12	13h10	13h13	13h15
$\hat{h}(cm)$ (9 ms)	53.22	53.05	53.00	53.06	53.15	53.04	53.09	53.71	54.66
$\hat{h}(cm)$ (20 ms)	53.27	53.02	53.01	53.06	53.32	53.04	53.21	53.31	54.26

We notice from Table 8 that for a length of integration of 9 ms, the standard deviation of $\hat{h}$ is 5.42 mm and the mean value of $\hat{h}$ is 53.33 cm. For a length of integration of 20 ms the standard deviation of $\hat{h}$ is 3.88 mm and the mean value of $\hat{h}$ is 53.28 cm. We conclude that the minimum length of integration defined by simulation is in agreement with the real case. The millimeter accuracy obtained in simulation is also achieved using real data, but with a degraded performance by a factor of an order of ~ 5. Several reasons can explain this difference. First, the horizontal geometry of the experimental setup is considered to be known, but with a limited accuracy. In addition, we do not take into consideration the external physical parameters such as the wind which can distort the experimental setup. Finally, the inaccuracies in the estimation of the GNSS signal parameters (code, phase and frequency) in the linear-circular model are not taken into consideration. We also do not take into account, in the derivation of our estimate, the correlation (the independence of the observations is assumed in expressions (4) and (20)) due to, for example, the limited band-pass of the GNSS receiver front-end.

5. Conclusion

In this article, a linear-circular estimate is proposed for data fusion. We estimate the intercept, the slope of the regression line and the noise power for each sensor. We assume that the noise on the angular measurements is distributed according to a von Mises distribution (Circular Normal distribution). The estimate is derived by maximizing the likelihood of the measurements provided by the sensors according to the linear-circular model. We show that the estimate is a weighted sum fusion operator of the observations in the circular domain. The proposed estimate is an iterative procedure that maximizes a periodic contrast function. We first derive the variance of the estimated slope in the multi-sensors case. Then, we show, in the context of an application where the predictors

are obtained as sufficiently precise floating-point data and the search window is well defined, that the contrast function has a single global maximum. The proposed estimate is first assessed using synthetic data. In the synthetic case, we show that the proposed estimator is a fusion operator performing similarly to the weighted sum fusion operator in the linear domain. The estimator is also assessed by processing the phase difference between GNSS signals provided by two antennas. The objective is to estimate the linear parameters of the phase difference in order to derive the height between two antennas. We show that the robustness of the height estimates and accuracy are improved when the observations obtained from several satellite signals are fused. Finally, the proposed estimator is assessed on real data. We show in this experimentation, that the theoretical study of the proposed estimator can be used to predict the length of integration of the signal necessary for obtaining an unbiased estimation and reach the millimeter accuracy for integration times of an order of tens of milliseconds. An extension of this article would be the joint estimation of the horizontal geometry of the setup as well as the height.

Acknowledgment

The authors would like to thank the CPER MARCO program for its financial support.

Appendix A. Derivation of the MLE estimate of β for unwrapped data

Let us define the expressions of $\hat{\alpha} + 2k\pi$ and $\hat{\beta}$ that maximize the likelihood function. $\hat{\alpha}$ is the solution of:

$$\frac{\partial\, L\,(Y^s)}{\partial \alpha} = 0$$

$$\left(\frac{1}{\sigma^s\,\sqrt{2\pi}}\right)^N \sum_{k=-\infty}^{\infty}\sum_{n=1}^{N}\frac{1}{(\sigma^s)^2}(y_n^s - \hat{\alpha} - 2k\pi - \beta\; x_n^s)\exp\left(-\frac{1}{2(\sigma^s)^2}\sum_{n=1}^{N}(y_n^s - \hat{\alpha} - 2k\pi - \beta\; x_n^s)^2\right) = 0$$

$$\Leftrightarrow \forall k, \sum_{n=1}^{N}(y_n^s - \hat{\alpha} - 2k\pi - \beta\; x_n^s) = 0 \tag{A.1}$$

$$\Leftrightarrow \hat{\alpha} + 2k\pi = \frac{\sum_{n=1}^{N} y_n^s - \beta\sum_{n=1}^{N} x_n^s}{N} \tag{A.2}$$

and $\hat{\beta}$ is the solution of :

$$\frac{\partial\, L\,(Y^s)}{\partial\beta} = 0$$

$$\left(\frac{1}{\sigma^s\,\sqrt{2\pi}}\right)^N \sum_{k=-\infty}^{\infty}\sum_{n=1}^{N}\frac{1}{\sigma^2}x_n^s(y_n^s-\hat{\alpha}-2k\pi-\hat{\beta}\;x_n^s)\exp\left(-\frac{1}{2(\sigma^s)^2}\sum_{n=1}^{N}(y_n^s-\hat{\alpha}-2k\pi-\hat{\beta}\;x_n^s)^2\right)=0$$

$$\Leftrightarrow \forall k, \sum_{n=1}^{N}(y_n^s\;x_n^s - x_n^s(\hat{\alpha}+2k\pi)-\hat{\beta}\;(x_n^s)^2)=0 \tag{A.3}$$

The expression of $\hat{\beta}$ is, as in the linear domain, given by:

$$\hat{\beta}=\frac{\sum_{n=1}^{N}(N\;y_n^s\;x_n^s)-\sum_{n=1}^{N}y_n^s\;\sum_{n=1}^{N}x_n^s}{\sum_{n=1}^{N}N\;(x_n^s)^2-\left(\sum_{n=1}^{N}x_n^s\right)^2} \tag{A.4}$$

In the multi-sensors case, each sensor is characterized by its noise power $-2ln(A(\kappa^s))$. The expression of $\hat{\beta}$ becomes:

$$\hat{\beta}=\frac{\sum_{s=1}^{S}\sum_{n=1}^{N}(N\;y_n^s\;x_n^s)-\sum_{s=1}^{S}\sum_{n=1}^{N}y_n^s\;\sum_{s=1}^{S}\sum_{n=1}^{N}x_n^s}{\sum_{s=1}^{S}\sum_{n=1}^{N}N\;(x_n^s)^2-\left(\sum_{s=1}^{S}\sum_{n=1}^{N}x_n^s\right)^2} \tag{A.5}$$

References

[1] S. R. Jammalamadaka, A. SenGupta, Topics in Circular Statistics, Vol. 5 of Series on Multivariate Analysis, World Scientific, 2001, 336pp.

[2] G. Stienne, S. Reboul, M. Azmani, J. Choquel, M. Benjelloun, A multi-temporal multi sensor circular fusion filter, Information Fusion 18 (2014) 86–100. doi:http://dx.doi.org/10.1016/j.inffus.2013.05.012.

[3] S. Reboul, M. Benjelloun, Joint segmentation of the wind speed and direction, Signal Processing 86 (4) (2006) 744 – 759. doi:https://doi.org/10.1016/j.sigpro.2005.07.014.
URL http://www.sciencedirect.com/science/article/pii/S0165168405002306

[4] A. G. Hussin, Hypothesis testing of parameters for ordinary linear circular regression, Pakistan Journal of Statistics and Operation Research 2 (2) (2006) 79–86.
URL http://www.pjsor.com/index.php/pjsor/article/view/90

[5] G. Stienne, S. Reboul, M. Azmani, J. B. Choquel, M. Benjelloun, GNSS dataless signal tracking with a delay semi-open loop and a phase open loop, Signal Processing 93 (5) (2013) 1192–1209. doi:http://dx.doi.org/10.1016/j.sigpro.2012.12.011.

[6] I. Marković, I. Petrović, Speaker localization and tracking with a microphone array on a mobile robot using von mises distribution and particle filtering, Robotics and Autonomous Systems 58 (11) (2010) 1185 – 1196. doi:https://doi.org/10.1016/j.robot.2010.08.001.
URL http://www.sciencedirect.com/science/article/pii/S0921889010001387

[7] P. E. Trahanias, D. Karakos, A. N. Venetsanopoulos, Directional processing of color images: theory and experimental results, IEEE Transactions on Image Processing 5 (6) (1996) 868–880. doi:10.1109/83.503905.

[8] N. I. Fisher, Statistical Analysis of Circular Data, Cambridge University Press, 1993. doi:10.1017/CBO9780511564345.

[9] K. Mardia, P. Jupp, Directional statistics, Wiley Series in Probability and Statistics, John Wiley and Sons Inc.: Chichester, UK, 1999.

[10] G. Kurz, I. Gilitschenski, U. D. Hanebeck, Recursive bayesian filtering in circular state spaces, IEEE Aerospace and Electronic Systems Magazine 31 (3) (2016) 70–87. doi:10.1109/MAES.2016.150083.

[11] G. Kurz, I. Gilitschenski, U. D. Hanebeck, Unscented von mises–fisher filtering, IEEE Signal Processing Letters 23 (4) (2016) 463–467.

[12] G. Stienne, S. Reboul, J. Choquel, M. Benjelloun, Cycle slip detection and repair with a circular on-line change-point detector, Signal Processing 100 (2014) 51 – 63. doi:https://doi.org/10.1016/j.sigpro.2014.01.003.
URL http://www.sciencedirect.com/science/article/pii/S0165168414000061

[13] K. El Mokhtari, S. Reboul, J. Choquel, G. Stienne, B. Amami, M. Benjelloun, Circular particle fusion filter applied to map matching, IET Intelligent Transport Systems 11 (8) (2017) 491–500.

[14] K. El Mokhtari, S. Reboul, J. Choquel, G. Stienne, B. Amami, M. Benjelloun, An imm filter defined in the linear-circular domain, application to maneuver detection with heading only, Mathematical Problems in Engineering 2018 (Article ID 3531075) (2018) 14 pages.

[15] I. Marković, J. Ćesić, I. Petrović, Von mises mixture phd filter, IEEE Signal Processing Letters 22 (12) (2015) 2229–2233. doi:10.1109/LSP.2015.2472962.

[16] A. L. Gould, A regression technique for angular variates, Biometrics 25 (4) (1969) 683–700.
URL http://www.jstor.org/stable/2528567

[17] R. A. Johnson, T. E. Wehrly, Some angular-linear distributions and related regression models, Journal of the American Statistical Association 73 (363) (1978) 602–606.
URL http://www.jstor.org/stable/2286608

[18] N. I. Fisher, A. J. Lee, Regression models for an angular response, Biometrics 48 (3) (1992) 665–677.

[19] B. Presnell, S. P. Morrison, R. C. Littell, Projected multivariate linear models for directional data, Journal of the American Statistical Association 93 (443) (1998) 1068–1077.
URL http://www.jstor.org/stable/2669850

[20] G. Nuñez-Antonio, E. Gutiérrez-Peña, G. Escarela, A bayesian regression model for circular data based on the projected normal distribution, Statistical Modelling 11 (3) (2011) 185–201. arXiv:https://doi.org/10.1177/1471082X1001100301, doi:10.1177/1471082X1001100301.
URL https://doi.org/10.1177/1471082X1001100301

[21] F. Wang, A. E. Gelfand, Directional data analysis under the general projected normal distribution, Statistical Methodology 10 (1) (2013) 113 – 127. doi:https://doi.org/10.1016/j.stamet.2012.07.005.
URL http://www.sciencedirect.com/science/article/pii/S1572312712000457

[22] A. E. Sikaroudi, C. Park, A mixture of linear-linear regression models for a linear-circular regression, Statistical Modelling 0 (0) (2019) 1471082X19881840. arXiv:https://doi.org/10.1177/1471082X19881840, doi:10.1177/1471082X19881840.

URL https://doi.org/10.1177/1471082X19881840

[23] M. A. Ribot, J.-C. Kucwaj, C. Botteron, S. Reboul, G. Stienne, J. Leclère, J.-B. Choquel, P.-A. Farine, M. Benjelloun, Normalized GNSS Interference Pattern Technique for Altimetry, Sensors 14 (6) (2014) 10234–10257. doi:10.3390/s140610234.

URL http://www.mdpi.com/1424-8220/14/6/10234

[24] G. Stienne, Traitement des signaux circulaires appliqués à l'altimétrie par la phase des signaux GNSS, Ph.D. thesis, Université du Littoral Côte d'Opale (12 2013).

[25] F. Gustafsson, Adaptive filtering and change detection, John Wiley and Sons, 2000.

[26] I. Oruç, L. T. Maloney, M. S. Landy, Weighted linear cue combination with possibly correlated error, Vision research 43 (23) (2003) 2451–2468.

[27] J. Cai, E. W. Grafarend, C. Hu, The statistical property of the gnss carrier phase observations and its effects on the hypothesis testing of the related estimators, in: Proceedings of the 20th International Technical Meeting of the Satellite Division of The Institute of Navigation (ION GNSS 2007), 2007, pp. 331–338.